Journal of Physics B: Atomic, Molecular and Optical Physics

TOPICAL REVIEW

# Correlated electron–nuclear dynamics of molecules in strong laser fields



To cite this article: Wenbin Zhang *et al* 2020 *J. Phys. B: At. Mol. Opt. Phys.* **53** 162001

IOP Publishing Journal of Physics B: Atomic, Molecular and Optical Physics
J. Phys. B: At. Mol. Opt. Phys. **53** (2020) 162001 (15pp) https://doi.org/10.1088/1361-6455/ab9763

## Topical Review

# Correlated electron–nuclear dynamics of molecules in strong laser fields

**Wenbin Zhang[1], Peifen Lu[1], Junyang Ma[1], Hui Li[1], Xiaochun Gong[1] and Jian Wu[1,2]**

[1] State Key Laboratory of Precision Spectroscopy, East China Normal University, Shanghai 200062, People's Republic of China
[2] Collaborative Innovation Center of Extreme Optics, Shanxi University, Taiyuan, Shanxi 030006, People's Republic of China

E-mail: jwu@phy.ecnu.edu.cn

Received 12 January 2020, revised 14 March 2020
Accepted for publication 28 May 2020
Published 30 June 2020

**Abstract**

For a molecule irradiated by an intense laser field, the sudden excitation or removal of an electron will trigger ultrafast electronic and nuclear dynamics, of which the timescales are usually several orders different and can be separately treated according to the Born–Oppenheimer approximation. However, the electrons and nuclei are intrinsically coupled in a molecule and should be considered on an equal footing in strong laser fields. In this paper, we review the recent progresses made on the correlated electron–nuclear dynamics of molecules exposed to strong laser fields, in particular, the multiphoton energy absorption and deposition in molecular dissociative ionization. Moreover, the electron–nuclear correlation offers an alternative visual angle to capture the fascinating strong-field molecular dynamics, including the photon-number-resolved asymmetric dissociative single ionization, high-order above-threshold dissociation, and Rydberg states excitation in dissociative frustrated ionization of molecules, which cannot be revealed if only the electrons or nuclear fragments are measured independently.

Keywords: strong-field molecular physics, electron–nuclear correlation, photon energy absorption and deposition, electron–ion coincidence measurement

(Some figures may appear in colour only in the online journal)

## 1. Introduction

The light–matter interaction has been the object of continuous research for a long time due to its potential applications in scrutinizing and understanding the microcosms of nature [1, 2]. With the advent of ultrafast laser technology and the development of advanced molecular imaging techniques, it is now possible to explore the rich dynamics in the chemical reactions on an atomic or molecular scale. Comparing with atoms, the interaction of molecules with intense laser pulses becomes more complicated because additional degrees of freedom associated with the nuclei will be involved, which however, offers richer perspectives on the strong-field molecular dynamics. A multitude of intriguing strong-field phenomena have been observed for molecules exposed to strong laser fields, such as the bond softening and hardening [3–6], above-threshold dissociation (ATD) [7–10], tunneling dissociation [11], directional bond breaking [12, 13], light-induced electron self-diffraction [14–16], high-harmonic generation [17, 18], charge-resonance-enhanced ionization (CREI) [19–22], and Rydberg states excitation in dissociative frustrated ionization [23–26]. The correlated electronic and nuclear dynamics jointly determine the ultimate fate of the molecules.

 

In general, owing to the lighter mass of the electron, the timescales of the electronic motion at sub-femtosecond or attosecond are much shorter than that of the nuclear motion which typically ranges from tens to hundreds of femtoseconds or even longer. Therefore, the dynamics of the electrons and nuclei of a molecule in the strong laser fields are usually separated according to the Born–Oppenheimer (BO) approximation. However, previous works [27–33] have shown that the electron and nuclear dynamics are actually coupled with each other during the light–molecule interaction. For instance, in the autoionization of highly excited molecules [28–31, 33], the nuclear motion on the strongly repulsive potential energy surface can be very fast while the sojourn time of the electron on excited state becomes relatively long, such that the electronic and nuclear motions occur on comparable timescales. In such cases, the strongly coupled non-BO electron–nuclear dynamics in the molecules must be considered. Actually, although the timescales of the electronic and nuclear dynamics are different in most cases, the electrons and nuclei are intrinsically coupled in the molecules and their correlation has played a crucial role in the strong-field dynamics of molecules.

Understanding the electron–nuclear correlation in molecules has long been an attractive topic in strong-field molecular physics, which can provide deeper insights of the molecular photoionization and fragmentation. The essential question is how the molecule absorbs the photon energy from the laser fields and partitions the energy among various degrees of freedom in the molecular system. For molecules, not only the electrons but also the additional vibrational, rotational and dissociative motions of the nuclei can serve as energy reservoirs. However, there is no direct coupling between the nuclei and the laser field for most of the homonuclear diatomic molecules because of the absence of permanent dipole moments. To deposit the photon energy into the nuclei, the laser fields should first couple energy to the electrons, and then the electrons transfer the gained photon energy to the nuclei via their correlated interactions. The electron–nuclear photon energy sharing dynamics can be revealed by tracing the strong-field dissociative ionization of the molecules.

A particularly powerful tool for investigating the electron–nuclear correlations in the photon energy sharing is the electron–nuclear joint energy spectrum (JES) [34]. In the JES, the dissociative ionization yield as a function of both the electronic and nuclear kinetic energies is plotted, which requires the coincident detection of both the electrons and nuclear fragments ejected from the same molecule. With the development of the multi-particle coincidence detection techniques [35], one is now able to measure the electrons and charged nuclei in coincidence. By using the electron–nuclear JES, the correlated electron–nuclear dynamics has been successfully investigated in the single-photon dissociative ionization of molecules induced by synchrotron radiation [29, 36, 37], where the absorbed photon energy is shared among the ejected electron and nuclear fragments. As compared to the case in the synchrotron radiation, the electron–nuclear correlated dynamics becomes much more intricate for molecules exposed to a strong laser fields where multiple photons are involved. In the presence of a strong laser field, the molecules may absorb multiple photons beyond the minimal number required for the ionization, leading to discrete energy peaks in the photoelectron spectrum spaced by the photon energy, which is referred to as above-threshold ionization (ATI) [38]. Following the ionization, the succeeding dissociation of the molecular ion accessed via bond softening and hardening [3–6] or ATD [7–10] will further result in interesting fine structures in the nuclear kinetic energy release (KER) spectra. With assistance of the electron–nuclear JES, the details of the correlated electron–nuclear dynamics in the strong-field dissociative ionization of molecules can be revealed.

For the case in intense laser fields, the correlation between the electrons and nuclei in the molecular dissociation has been theoretically studied for the simplest $H_2^+$ molecules [39–46]. It was predicted [39] that the ejected electron in the strong-field multiphoton dissociative ionization of $H_2^+$ will share parts of the absorbed photon energy with the nuclei via their correlated interaction. The sum of the electron energy $E_e$ and nuclear energy $E_N$ can be described as $E_N + E_e = n\hbar\omega - I_{p0} - U_p$ (atomic units were used throughout, unless indicated otherwise), with $n$ the number of absorbed photons, $\omega$ the laser frequency, $I_{p0}$ the ionization potential and $U_p$ the ponderomotive energy, respectively. Generally, the correlated sharing of the multiphoton energy between the electrons and nuclei manifests itself as the multiple photon-energy-spaced diagonal lines in the electron–nuclear JES [39–46]. On the other hand, for the case close to tunneling regime, it was found that the electron does not share the photon energy with the nuclei [40]. The distinct energy-sharing mechanisms in the multiphoton and tunneling regimes were investigated by using an energy-resolved population imaging method [42]. Moreover, the inter- and intracycle interference effects were identified in the strong-field dissociative ionization of $H_2^+$ [46], which further enrich the structures of the electron–nuclear JES. The theoretical predictions [39, 40, 42, 45, 46] made on the electron–nuclear energy sharing suggest that the correlation between electron and nuclear dynamics in strong-field breaking of molecules is more complex than one would have anticipated, which strongly motivate experimental progresses on the correlated dynamics in dissociative ionization of molecules.

The experimental studies of the strong-field dissociative ionization of molecules greatly benefit from the development of the multi-particle coincidence measurement technology [34], with which the electrons and ions produced from the molecular fragmentation can be measured in coincidence. Using a reaction microscope of cold target recoil-ion momentum spectroscopy (COLTRIMS) [34, 35], Wu *et al* [47] experimentally explored the electron–nuclear correlated photon energy sharing dynamics in the above-threshold multiphoton dissociative single ionization of the $H_2$ molecule exposed to intense femtosecond laser pulses. Multiple diagonal lines were experimentally observed in the electron–nuclear JES, evidently reflecting the correlated sharing of the absorbed photon energy between the emitted electron and nuclear fragments. Inspired by this study, several experimental investigations on

the electron–nuclear correlated dynamics in strong-field dissociative ionization of molecules have appeared [48–53], in particular, the correlated photon energy absorption and deposition. As the primary stage of light–molecule interaction, the multiphoton energy absorption and deposition governs the succeeding photon-induced molecular dynamics and thus the ultimate fate of the molecule, including the asymmetric dissociative single ionization [50], the high-order ATD [51], and the Rydberg states excitation in dissociative frustrated ionization of molecules [53]. The recent progresses on the electron–nuclear correlated dynamics of molecules in the strong laser fields will be reviewed in the following sections.

## 2. Theoretical modeling

Before go to the experimental progresses, we would like to briefly review the theoretical modeling of the correlated electron–nuclear dynamics, in particular the electron–nuclear energy sharing in dissociative ionization of the simplest $H_2^+$ molecules [39–46]. Generally, the correlated electron–nuclear dynamics in dissociative ionization of $H_2^+$ can be revealed by numerically solving the time-dependent Schrödinger equation (TDSE) with the reduced-dimensionality model. In this model of $H_2^+$, the electronic and nuclear degrees of freedom are exactly treated within one-dimension aligned with the linearly polarized laser pulse which is parallel to the molecular axis. In terms of the coordinates of the nuclei, i.e., the internuclear separation $R$, and the electronic coordinate $x$ measured from the mass center of two nuclei in the direction of the laser polarization axis, the length-gauge TDSE for $H_2^+$ molecule can be written as (atomic units are used throughout) [41, 45, 46],

$$\begin{aligned} \mathrm{i}\frac{\partial}{\partial t}\Psi(R,x;t) &= H(t)\Psi(R,x;t) \\ &= [H_{\mathrm{N}} + H_{\mathrm{e}} + V_{\mathrm{eN}} + V_{\mathrm{N}} + \mathcal{E}(t)x]\Psi(R,x;t), \end{aligned}$$

where the Hamiltonian includes several terms. $H_{\mathrm{N}} = -(1/m_{\mathrm{p}})\partial^2/\partial R^2$ is the nuclear kinetic energy with proton mass of $m_{\mathrm{p}}$, $H_{\mathrm{e}} = -(1/\mu_{\mathrm{e}})\partial^2/\partial x^2$ is the electronic kinetic energy with reduced electron mass of $\mu_{\mathrm{e}}$, $V_{\mathrm{eN}} = -1/\sqrt{(x-R/2)^2+a(R)} - 1/\sqrt{(x+R/2)^2+a(R)}$ is the electron–nuclei Coulomb interaction with modified soft-core parameter of $a(R)$ [54] aiming in producing the full-dimensional $1s\sigma_{\mathrm{g}}$ BO potential, $V_{\mathrm{N}} = 1/R$ is the Coulomb repulsion of the two protons, $\varepsilon(t) = \varepsilon_0 \exp[-2\ln 2(t/\tau_0)^2]\cos(\omega_0 t)$ is the employed laser field with $\varepsilon_0$, $\tau_0$, and $\omega_0$ being the peak electric-field amplitude, pulse duration and center frequency, respectively.

Based on the numerical solution of the TDSE accessed by using Crank–Nicolson split-operator method, the physical observable of electron–nuclear JES can be extracted by employing different energy analysis methods. For instance, in reference [39] the electron–nuclear energy sharing is mapped by tracing the probability of the correlated electron–nuclear wave packet with nuclear energy of $E_{\mathrm{N}}$ and electron energy of $E_{\mathrm{e}}$, which can be expressed as $P(E_{\mathrm{N}}, \mathrm{E_e}) = \sum_{l=\mathrm{g,u}} \left|\psi^l_{E_{\mathrm{N}},E_{\mathrm{e}}}|\Psi(t)\right|^2$. Here $l$ = g, u denote the gerade and ungerade symmetries of the wave packets, respectively, and the $\psi^l_{E_{\mathrm{N}},E_{\mathrm{e}}}$ is the wave function of the double continuum scattering state, i.e., $\psi^l_{E_{\mathrm{N}},E_{\mathrm{e}}}(R,x) = \psi_{E_{\mathrm{N}}}(R)\psi^l_{,E_{\mathrm{e}}}(R;x)$. On the other hand, the electron–nuclear JES of $H_2^+$ can also be extracted by employing the molecular resolvent operator method [40, 42, 43, 45] and the time-dependent surface flux method [41, 44, 46]. Moreover, the strong field approximation model including nuclear kinetic energy was employed to understand the rich inter- and intra-cycle interference structures in the electron–nuclear JES [46].

## 3. Experimental method: multi-particle coincidence measurements using femto-COLTRIMS

Experimentally, to access the ultrafast electronic and nuclear dynamics of molecules in strong laser fields, both the ultrashort intense laser pulses and the molecular imaging techniques are required. This can be achieved by the combination of a titanium-doped sapphire (Ti:sapphire) multipass amplifier laser system and an ultrahigh-vacuum reaction microscope of COLTRIMS [34, 35], which is referred to as femto-COLTRIMS apparatus. The Ti:sapphire laser system generates laser pulses with wavelength centered at 790 nm, pulse durations of tens femtoseconds (e.g. 25 fs), and repetition rate of 10 kHz. The COLTRIMS is capable of measuring the three-dimensional momenta of electron and nuclear fragments in coincidence, which can therefore provide very rich information about the ultrafast dynamics of molecules.

The simplified layout of the femto-COLTRIMS apparatus is schematically shown in figure 1. The intense near-infrared (IR) femtosecond laser pulses from the multipass amplifier Ti:sapphire laser system can be controlled in the time-frequency domain for different experimental purposes. For example, as illustrated in figure 1, the IR laser pulses derived from the laser system can be frequency doubled in a $\beta$-barium borate ($\beta$-BBO) crystal to produce ultraviolet (UV) pulses centered at 395 nm for the study of photon energy sharing in multiphoton ionization regime [47–50, 53]. The laser pulses were sent into the vacuum chamber through a viewport and then tightly focused onto a molecular beam using a concave silver mirror ($f$ = 75 mm) inside the COLTRIMS apparatus. The molecular beam propagating along the $y$-axis was generated using a supersonic gas jet. The employment of the supersonic diffuse gas jets can produce well localized and internally cold molecular targets for high-resolution electron- and ion-momentum measurements.

The measurements were performed in a reaction microscope of COLTRIMS, as schematically illustrated in figure 1, where not only the charged ions and electrons but also the excited neutral Rydberg atoms ejected from the same molecule can be detected in coincidence by using two time- and position-sensitive microchannel plate (MCP) detectors mounted on two opposite sides of the spectrometer. The weak homogeneous electric field ($E$-field) and magnetic field ($B$-field) were utilized to guide the generated ions and

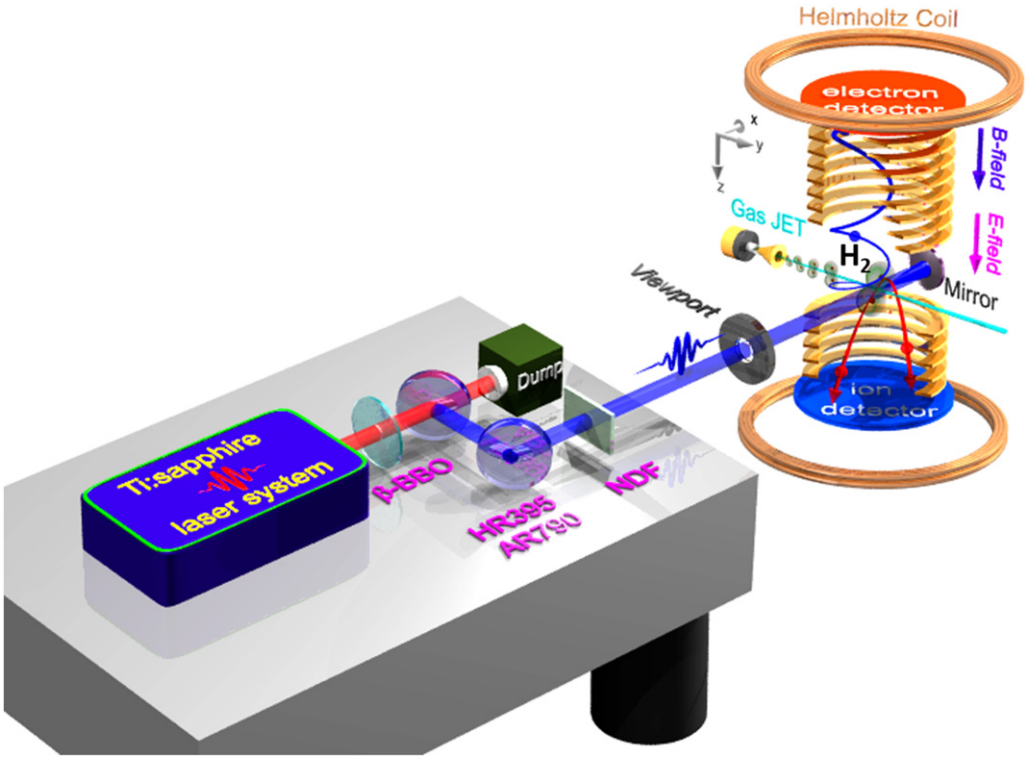


**Figure 1.** Schematic diagram of the femto-COLTRIMS apparatus. The exhibited layout illustrates the generation of linearly polarized UV pulses for interacting with $H_2$ molecules in the vacuum chamber.

electrons towards the corresponding detectors. On the other hand, the produced excited neutral Rydberg atoms can also be detected if they fly towards the ion detector and impinges on the detector with an internal potential energy larger than the work function of the MCP (a few eV). It thus allows us to investigate the dynamics of the Rydberg states excitation in strong-field dissociation of molecules [23, 25, 26, 53]. The three-dimensional momenta of the detected particles were reconstructed from the measured time-of-flights (TOFs) and positions of the impacts during the offline analysis.

## 4. Electron–nuclear energy sharing in multiphoton dissociative single ionization of molecules

In this section, the photon energy sharing between the ejected electron and nuclei in the above-threshold multiphoton dissociative single ionization of the simplest two-electron system $H_2$ [47] and multielectronic system CO [48] molecules are discussed. With assistance of the electron–nuclear JES, we also show in the following the crucial role of the electron–nuclear correlation in the photon-number-dependent asymmetric dissociative single ionization [50] and the electron-rescattering induced high-order ATD [51] of molecules, which cannot be revealed if the freed electron is not measured in coincidence with the nuclear fragments.

### *4.1. Two-electron system: $H_2$*

As the simplest neutral molecule, the hydrogen molecule serves as a prototypical system for exploring the numerous fundamental phenomena. Stimulated by the theoretical prediction of electron–nuclear photon energy sharing in multiphoton dissociative ionization of $H_2^+$ [39], the first experimental test on this problem was carried out in the above-threshold multiphoton dissociative single ionization of $H_2$, i.e., $H_2 + n\omega \rightarrow H^+ + H + e$ referred to as ($H^+$, H) channel, driven by a UV femtosecond laser pulse [47]. Figure 2(a) displays the measured electron–nuclear JES of the ($H^+$, H) channel. Similar to the predicted features in references [39, 40], multiple diagonal lines separated by the photon energy were clearly observed in the electron–nuclear JES, indicating correlated sharing of the absorbed photon energy among the ejected electrons and nuclei in the above-threshold dissociative ionization of $H_2$. According to the energy conservation law, along each diagonal line the electron energy $E_e$ decreases with the increase of the nuclear energy $E_N$, because their sum energy $E_{sum} = E_N + E_e$ is a constant. The corresponding energy spectra of the nuclei $E_N$, electron $E_e$ and their sum $E_{sum}$, are shown in figures 2(b)–(d), respectively. As shown in figure 2(c), the electron energy spectrum is modulated with rich fine structures as compared to the nuclear energy spectrum in figure 2(b). The fine structures in the $E_e$ spectrum are polarization-dependent and disappear in the circularly polarized laser pulses because of the suppression of the Freeman resonances [55, 56]. Interestingly, by considering total energies of all the ejected fragment particles, clear discrete photon-energy-spaced ATI peaks were reconstructed in the $E_{sum}$ spectrum as shown in figure 2(d), which further highlights the fact that the electrons and nuclei of the molecule as a whole absorbs the photon energy from the light.

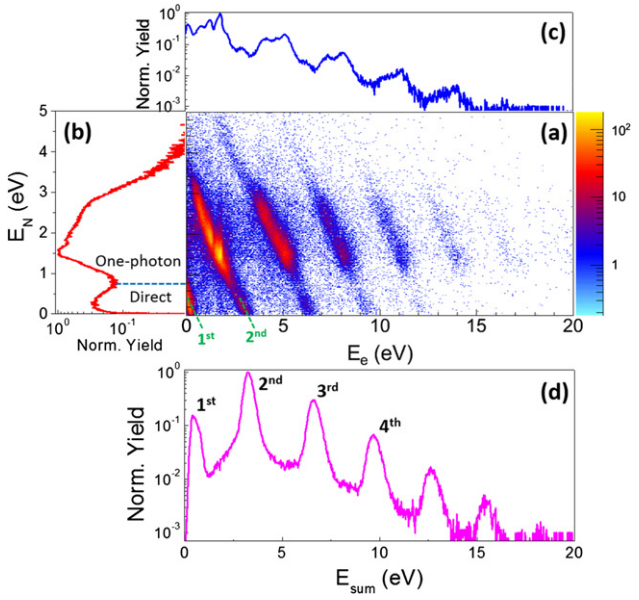


**Figure 2.** (a) Measured electron–nuclear correlated JES of ($H^+$, H) channel in a linearly polarized UV pulses with peak intensity of $4.3 \times 10^{13}$ W cm$^{-2}$. The corresponding spectra of the (b) nuclear energy $E_N$, (c) photoelectron energy $E_e$ and (d) their sum-energy $E_{sum}$. Reprinted figure with permission from [47], Copyright 2013 by the American Physical Society.

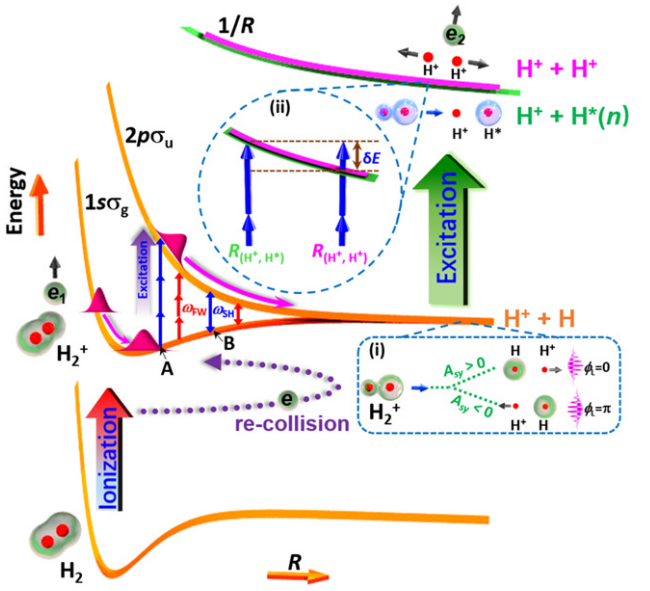


**Figure 3.** Schematic diagram showing the molecular dynamics involved in the strong-field dissociative ionization of a $H_2$ molecule, including the above-threshold dissociative single ionization, Coulomb-exploded double ionization, electron-rescattering assisted high-order ATD, asymmetric dissociative single ionization, and Rydberg state excitation in dissociative FDI of molecules. The $\omega_{FW}$ and $\omega_{SH}$ denote the laser frequency of the FW and SH wave components of the two-color laser pulses, respectively. The inset (i) illustrates the directional proton emission depending on the phase of the two-color laser field in dissociative single ionization of $H_2$. The inset (ii) sketchs the excitation of the stretching $H_2^+$ occuring at slightly different internuclear distances, where the molecular ion were resonantly tranferred onto the repulsive Rydbergs states at a smaller internuclear distance of $R_{(H+,H^*)}$, leading to a larger kinetic energy of the nuclear fragments of the ($H^+$, $H^*$) channel than those of the ($H^+$, $H^+$) channel for which the excess photon energy of $\delta E$ above the ionization threshold electron.

Driven by a strong UV laser field, the dissociative single ionization of $H_2$ molecule generally proceeds in two steps, as illustrated in figure 3. In the first step, one electron is released from the $H_2$ molecule and a nuclear wave packet (NWP) is launched on the ground state of $H_2^+$. In the second step, the laser-created $H_2^+$ dissociates into the continuum of a proton $H^+$ and a hydrogen atom H via direct pathway (stretching to the continuum of $H^+ + H$ along $1s\sigma_g$ state) or one photon pathway (stretching to the continuum of $H^+ + H$ along $2p\sigma_u$ state after resonantly absorbing one additional photon). As marked by the dashed line in figure 2(c), the low and high $E_N$ in the nuclear energy spectrum are correspondingly produced by the dissociation via the direct and one-photon pathways, respectively. As displayed in figure 2(a), for the 1st ATI peak where the dissociation is dominated by the direct pathway, almost all the excess photon energy is transferred to the nuclei while the electron is almost rest. However, for the 2nd ATI peaks in figure 2(a) where the one-photon dissociation pathway is predominant, most energy of the absorbed photons above the ionization threshold is taken by the electron in the ionization step, while the observed kinetic energy of the nuclei gains mainly from the succeeding photon-coupled transition and propagation on the potential energy curves. The dissociation dynamics of the molecule is determined by the amount of energy transferred to the nuclei in the first ionization step.

### *4.2. Multielectron molecule: CO*

Most previous studies on the electron–nuclear energy sharing were carried out for the simplest one- or two-electron systems of $H_2^+$ [39–46] and $H_2$ [47, 49, 51–53]. For the multi-electron molecules, the participation of multiple orbitals and numerous electronic states in the ionization and dissociation process will complicate the photon energy sharing dynamics. In a recent experiment, the energy correlation between the emitted electrons and ions in dissociative double ionization of a polyatomic hydrocarbon molecule of $C_2H_2$ was found to be negligible [57]. It further raises several questions that does the electron–nuclear photon energy sharing phenomena still holds in other multi-electron molecules besides the one- or two-electron systems of $H_2^+$ and $H_2$? and how does the multiple orbitals and electronic states of the molecule affect the energy partitions law? and what is the underlying mechanism that governs the photon energy sharing?

More recently, using CO as a prototype, the electron–nuclear sharing of the excess photon energy in above threshold multiphoton dissociative single ionization of multi-electron molecule was experimentally observed [48, 49]. Figure 4(a) displays the measured electron–nuclear JES of the multiphoton dissociative single ionization of CO molecules [48], i.e., CO + $n\omega \rightarrow C^+ + O + e$ [labeled as ($C^+$, O)], where the general feature of photon energy spaced diagonal lines are observed.

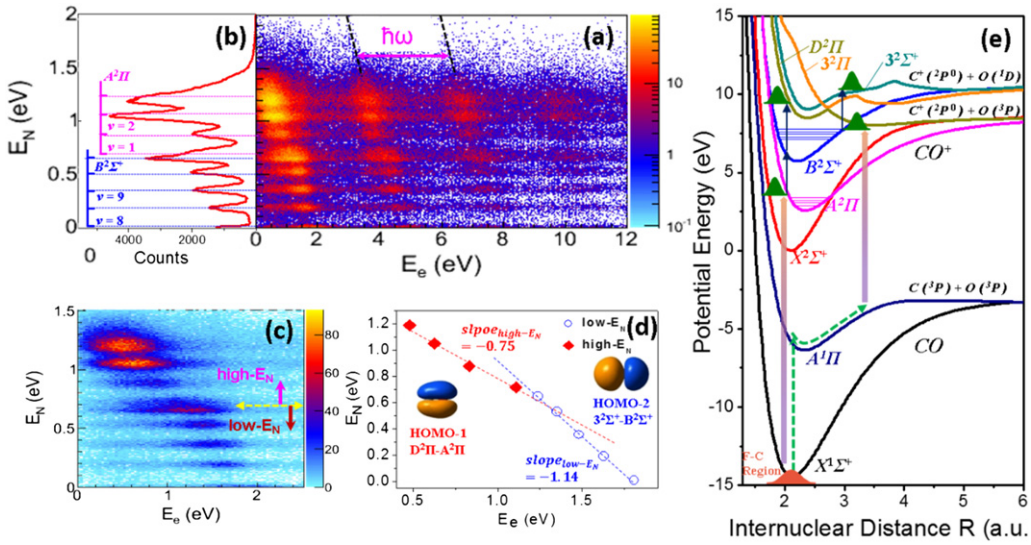


**Figure 4.** (a) Measured electron–nuclear JES of the ($C^+$, O) channel in a linearly polarized UV femtosecond laser pulse with peak intensity of $7.6 \times 10^{13}$ W cm$^{-2}$. (b) The corresponding nuclear KER spectra $E_N$ integrated over $E_e$. The locations of the expected $E_N$ of the photon coupled transitions starting from different vibrational levels in $B^2\Sigma^+$ and $A^2\Pi$ state are marked, respectively. (c) Enlarged JES distribution of the first diagonal line in (a). (d) Distributions of the energy peaks of the discrete JES islands in (c). Two JES structures in the low- and high-$E_N$ regions show different photon energy sharing slopes, which results from participation of different orbitals in the dissociative ionization process. (e) The relevant potential energy surfaces of CO and $CO^+$ showing the different pathways accessing for the dissociative single ionization of CO molecules. Adapted figures with permission from [48], copyright 2016 by American Physical Society.

As compared to the $H_2^+$ [39–46] and $H_2$ [47, 50–53], because of the complexity of the multi-electron system, the JES for the dissociative ionization of CO exhibits more features [48]. First of all, as shown in figure 4(b), the nuclear energy spectrum $E_N$ is featured with discrete fine structure, which maps the rich vibrational structure of the photoionization-created $CO^+$. The population of numerous vibrational states of the molecular cation in the ionization process provides the energy reservoir for the nuclei to store the gained photon energy. It is the key point for the above-observed electron–nuclear sharing of the absorbed photon energy. Moreover, as shown in figure 4(c), two sets of electron–nuclear energy sharing structures are observed in the enlarged distribution of the first diagonal line of the JES and can be distinguished as the low-$E_N$ ($E_N < 0.7$ eV) and high-$E_N$ ($E_N > 0.7$ eV), respectively. Figure 4(d) shows the peak energies of the discrete islands in the first diagonal line of the JES. The different slopes in the low- (slope $\sim -1.14$) and the high-$E_N$ (slope $\sim -0.75$) regions of the JES structure result from the participation of multiple orbitals and electronic states in the strong-field dissociative ionization process. By matching the vibrational energy space of various electronic states and the simulated final nuclear kinetic energy $E_N$ gained from different photon-coupled transitions processes, two dissociation pathways were identified in producing the low- and high-$E_N$ regions. As illustrated in figure 4(e), the observed low-$E_N$ events can be attributed to the two-photon coupled transition of the NWP from $B^2\Sigma^+$ state to the $3^2\Sigma^+$ and $3^2\Pi^+$ states, followed by dissociation into the $C^+(^2P^0) + O(^1D)$ limit; while the high-$E_N$ region is accessed via one-photon transition from the $A^2\Pi$ state to the $D^2\Pi$ state and followed by dissociation to the limit of $C^+(^2P^0) + O(^3P)$. For this two dissociation pathways, the dependences of the energy differences between the coupled electronic states on the internuclear distance are different, which lead to different slopes in the orbital-resolved JES and thus alter the electron–nuclear energy sharing process.

We note that the role of electron–nuclear correlation should be more significant in the strong-field dynamics of polyatomic molecules as compared to the diatomic molecules. In the dissociative ionization of the acetylene molecules, negligible photon energy sharing was found [57]. It is mainly because of that the acetylene molecule is not completely fragmentized into atomic fragments and part of the absorbed photon energy may be deposited into the excited (ro-)vibrational states of the survived molecular fragments which cannot be retrieved from our measurements. More efforts, both experimentally and theoretically, are demanded to reveal the rich dynamics.

### *4.3. Photon-number-resolved directional bond breaking of $H_2$ molecules*

For a molecule exposed to an intense laser field, the deposition of the absorbed photon energy into the electronic and nuclear degrees of freedom triggers the subsequent molecular dynamics, for instance, the directional bond breaking in dissociative single ionization of molecules. The directional breaking of the molecular bond in dissociative single ionization of hydrogen molecules has been extensively studied [12, 13, 58–73] by using asymmetric phase-controlled few-cycle [12, 58–63] or two-color [64–72] femtosecond laser pulses. In general, the directional bond breaking in molecular dissociative ionization is revealed by tracing the asymmetric

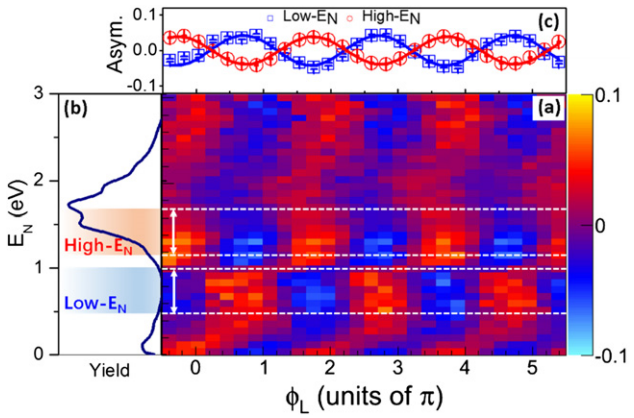


**Figure 5.** (a) Two-dimensional spectrum of the asymmetry parameter measured in the asymmetric dissociative single ionization of $H_2$ molecule driven by a phase-controlled two-color laser fields. The peak intensity of the employed FW and SH wave component is $I_{FW} \sim 1.2 \times 10^{13}$ W cm$^{-2}$ and $I_{SH} \sim 3.3 \times 10^{13}$ W cm$^{-2}$, respectively. The asymmetry parameter is quantitatively defined as $A(E_N, \phi_L) = [Y(E_N, \phi_L) - Y(E_N, \phi_L + \pi)]/[Y(E_N, \phi_L) + Y(E_N, \phi_L + \pi)]$, where $Y(E_N, \phi_L)$ is the $H^+$ yield as a function of nuclear kinetic energy $E_N$ and relative phase $\phi_L$ of the two-color laser pulse. (b) The corresponding $E_N$ spectrum integrated over the phase $\phi_L$ and electron energy $E_e$. (c) Asymmetry parameter of the low-$E_N$ (0.4 eV $< E_N <$ 0.9 eV) and high-$E_N$ (1.1 eV $< E_N <$ 1.6 eV) regions as indicated in (b). The solid sinusoidal curves are the numerical fits of the measured data. Adapted figures with permission from [50], copyright 2017 by American Physical Society.

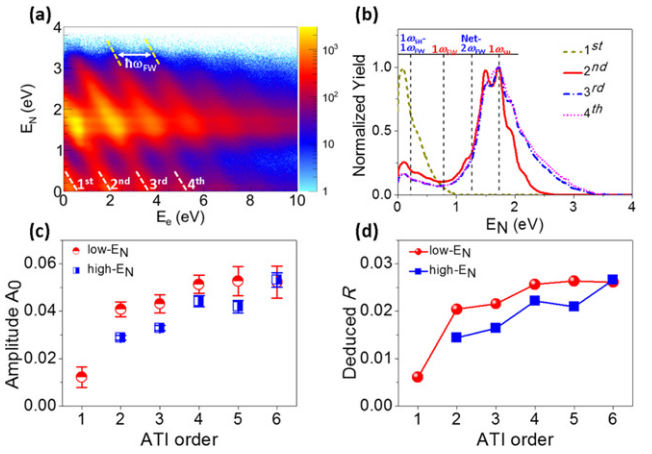


**Figure 6.** (a) Measured phase-integrated electron–nuclear JES of the ($H^+$, H) channel. (b) The normalized $E_N$ distributions by projecting on $E_e$ for the first four diagonal energy conservation lines as labeled in (a). The vertical dashed lines mark the expected locations of the $E_N$ for four dissociation pathways. (c) The ATI-order (photon number)-dependent fitted asymmetry amplitude $A_0$ of the ($H^+$, H) channel in low-$E_N$ (red circles) and high-$E_N$ (blue squares) regions. (d) The corresponding deduced relative weight (R) of various dissociation pathways as a function of each line order (ATI order) of the JES. Adapted figures with permission from [50], copyright 2017 by American Physical Society.

emission of electrons or nuclear fragments. Figure 5(a) displays the measured two-dimensional (2D) asymmetry spectrum of the proton emission in dissociative single ionization of $H_2$, i.e., the ($H^+$, H) channel, driven by a phase-controlled two-color laser field [50]. The asymmetric ion emission is interpreted as the interference of quantum pathways ending with opposite parities by absorbing and emitting different numbers of photons in the dissociation process [73]. As illustrated in figure 3, driven by a two-color field composing of the fundamental wave (FW) and its second harmonic (SH), several dissociation pathways [74–77, 79], e.g., $1\omega_{SH}$–$1\omega_{FW}$, $1\omega_{FW}$, net-$2\omega_{FW}$, $1\omega_{SH}$, $1\omega_{SH}$+$2\omega_{FW}$–$1\omega_{FW}$, and $3\omega_{FW}$ pathways, may contribute to the interference in the regions where their final kinetic energies are overlapped. The observed asymmetry at different energies of the $E_N$ spectrum indicates the participation of different dissociation pathways. As marked by the white dashed lines in figure 5(a), the low-$E_N$ (0.4 eV $< E_N <$ 0.9 eV) and high-$E_N$ (1.1 eV $< E_N <$ 1.6 eV) regions exhibit different asymmetries of the proton emission, which originate from the interference between the $1\omega_{FW}$ and $1\omega_{SH}$–$1\omega_{FW}$ pathways, and between the $1\omega_{SH}$ and net-$2\omega_{FW}$ pathways, respectively.

By taking advantage of the electron–nuclear JES, the dependence of the asymmetric proton emission on the total number of photons absorbed by the molecule can be revealed [50]. Figure 6(a) displays the $\phi_L$-integrated electron–nuclear JES of the ($H^+$, H) channel driven by the two-color laser pulses. In the JES, the multiple diagonal line spaced by the photon energy of the FW field ($\hbar\omega_{FW}$) allows one to unambiguously count the total number of photon energy absorbed by the molecule. Figure 6(b) plots the normalized $E_N$ spectrum integrated over $E_e$ for each one of first four diagonal lines (ATI order) in the JES. As compared to the $E_N$ spectrum integrated over the entire $E_e$, as displayed in figure 5(b), the $E_N$ spectrum corresponding to a single ATI order can reveal the relative weight of the above-mentioned four dissociation pathways. For instance, the $E_N$ spectrum is dominated by the $1\omega_{SH}$–$1\omega_{FW}$ for the first ATI order, while the higher-$E_N$ pathways, i.e., $1\omega_{FW}$, $1\omega_{SH}$, and net-$2\omega_{FW}$, becomes accessible with increased proportions for the higher ATI orders. The channel opening of the dissociation pathways with higher $E_N$ results from the deposition of more photon energies into the nuclei when more photons are absorbed by the molecule.

Since the asymmetric proton emissions are induced by the interference of various pathways with opposite parities, the ultimate asymmetry are thus related to the photon-number-dependent accessibility of the involved interfering pathways. Figure 5(c) plots the phase-dependent asymmetries of the low- and high-$E_N$ regions, where the solid curves are the numerical fits of the measured data by using the function of $A = A_0 \cos(\phi_L + \varphi_{A0})$ with $A_0$ and $\varphi_{A0}$ the amplitude and phase offset of the asymmetry, respectively. Interestingly, as shown in figure 6(c), the fitted amplitudes $A_0$ of the asymmetry for various ATI orders of the low- and high-$E_N$ regions increases with the increase of the ATI order. On the other hand, the asymmetry parameter $A_c$ for the pathway interference can be expressed as $A_c = [2R/(R^2 + 1)]\cos(\Delta\varphi)$ in a semiclassical model [13], where $R$ is the relative weight between the interfering pathways and $\Delta\varphi$ is the phase difference of the NWP accumulated during the dissociation via the two different pathways. By assuming that the $A_0$ of the fitting function equals the amplitude of the asymmetry parameter of the semiclassical model,

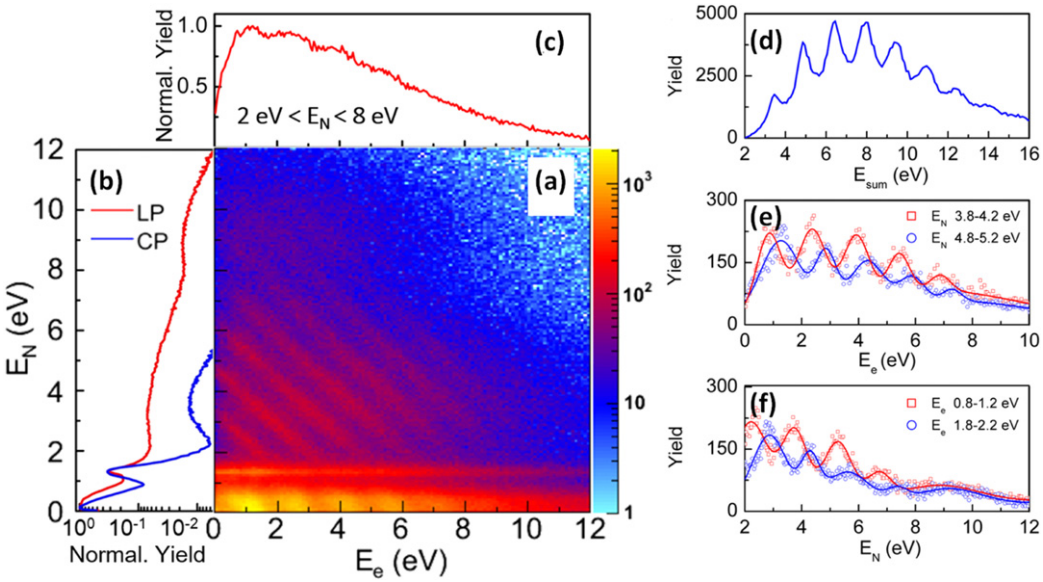


**Figure 7.** (a) Electron–nuclear JES of the above-threshold dissociative single ionization channel of ($H^+$, H) driven by linearly polarized near-IR (790 nm) laser pulses with a peak intensity of $I_0 = 9.0 \times 10^{13}$ W cm$^{-2}$. (b) Measured $E_e$-integrated nuclear energy spectra $E_N$ by linearly polarized (LP, red curve) and circularly polarized (CP, blue curve, $I_0 = 1.8 \times 10^{14}$ W cm$^{-2}$) laser pulses. (c) The photoelectron energy spectrum integrated over $E_N$ in the range of 2–8 eV in linearly polarized pulse. (d) The corresponding total energy spectrum of the coincidently measured nuclei and electron of the ($H^+$, H) channel by integrating the diagonal lines of the JES with $E_N$ ranging from 2 eV to 8 eV. (e) The integrated ATI spectra $E_e$ of the photoelectron obtained by fixing the $E_N$ in the ranges of 3.8–4.2 eV and 4.8–5.2 eV. (f) The integrated ATD spectra $E_N$ of the nuclear fragments obtained by fixing the $E_e$ in the ranges of 0.8–1.2 eV and 1.8–2.2 eV. Reproduced with permission from [51]. 2018.

i.e., $2R/(R^2 + 1) = A_0$, the relative weight $R$ between the dissociation pathways involved in the interference for the low- and high-$E_N$ regions can thus be deduced. As shown in figure 6(d), the deduced $R$ are featured with a similar dependence on the ATI orders as that of the amplitude $A_0$. The tendency of the invariable $R$ for the high ATI order is because of that all the possible dissociation channels are accessed with almost saturate probability when the molecule absorbs many photons from the laser fields.

### *4.4. High-order ATD of molecules assisted by electron–ion rescattering*

When multiple photons are absorbed by the molecules in strong laser fields, the ATD generally occurs in dissociative single ionization process [7–10]. In the ATD, multiple photons exceeding the binding energy of the molecular bond are deposited into the nuclei of molecules, leading to discrete photon-energy-spaced peaks in the KER spectra of the nuclear fragments. Since the first theoretical prediction of the ATD for the simplest $H_2^+$ molecules made more than twenty years ago [7], many efforts have been dedicated in observing the molecular ATD in strong laser field [8–10]. However, the experimental evidences of distinct high-order (more than three orders) ATD have never been reported, where the key problem of which lies on the electron–nuclear correlation in molecular dissociative ionization. To reveal the general feature of the high-order ATD, the coincidence measurements of the freed electron and nuclear fragments are required because the absorbed multiple photon energies are shared among the electronic and nuclear degrees of freedom.

Recently, a conclusive experimental observation of the high-order ATD of $H_2$ in strong laser fields was demonstrated [51] by employing the JES of the coincidently measured electron and nuclei ejected from the same molecule [47–53]. Differing from the aforementioned dissociative single ionization of $H_2$ accessed via the photon-coupled (one-photon, net-two-photon or three-photon) dipole transitions between the $1s\sigma_g$ and $2p\sigma_u$ state of $H_2^+$ [3, 10], the here-observed high-order ATD of $H_2$ [51] is assisted by the field-driven inelastic rescattering of the tunneled electrons. The electron rescattering-assisted high-order ATD of $H_2$ molecule is illustrated in figure 3. After interacting with intense laser fields, the neutral $H_2$ molecule emits one electron and launches an NWP on the $1s\sigma_g$ state of $H_2^+$. Then, the created NWP starts to move along the potential curve of $1s\sigma_g$ state, while the liberated electron is accelerated by the remaining oscillating laser fields to gain multiphoton energy. The energetic electron may be driven back to the parent ion and transfer the absorbed photon energy to the stretching $H_2^+$ by exciting the NWP onto the $2p\sigma_u$ state, resulting in the subsequent dissociation into nuclear fragments ($H^+$ and H) with high kinetic energies. Figure 7(a) displays the measured electron–nuclear JES of the ($H^+$, H) channel in linearly polarized 790 nm laser pulses [51]. The correlated photon energy sharing dynamics of the released electron and nuclei in the high-order ATD are bridged by the laser-driven inelastic electron rescattering, which can be revealed by the diagonal energy correlation lines in the high-$E_N$ ($E_N > 2$ eV) region

of the JES. As shown in figure 7(b), the relatively suppressed high-$E_N$ yield for the circularly polarized laser pulses verify the rescattering nature in producing the high-$E_N$ region, while the polarization-independent signals in the low-$E_N$ ($E_N < 2$ eV) region are mainly produced from the one-photon and net-two-photon dipole transitions between the $1s\sigma_g$ and $2p\sigma_u$ state of $H_2^+$ [3, 10].

Basing on the quantized photon nature of the incident light, it is logical for the observation of discrete photon-energy-spaced peaks in both the high-order ATD spectra of the nuclei and the ATI spectra of the photoelectron, since both the electron and nuclei can store multiple photon energy. As displayed in figures 7(b) and (c), the photon-energy-modulated structures are obscured in the sole nuclear or the photoelectron spectra of the high-$E_N$ region, which however, can be reconstructed in the total energy spectrum of the ejected electron and nuclear fragments, i.e., the $E_{sum}$ spectrum as shown in figure 7(d). Each peak in the $E_{sum}$ spectra corresponds to one diagonal line in the high-$E_N$ region of the JES. The ATI of the photoelectron and ATD of the nuclei are entangled because of the interference of the periodically emitted correlated electron–nuclear wave-packet in each optical cycle. Interestingly, as shown in figures 7(e) and (f), the discrete ATI (ATD) peaks in the photoelectron (nuclei) can be clearly reproduced by fixing the nuclear (photoelectron) energy. In analogy to the ATI photoelectron spectrum, more than four distinct photon-energy-spaced peaks are observed in the nuclear KER spectrum, which is an unambiguous evidence of the observation of the high-order ATD.

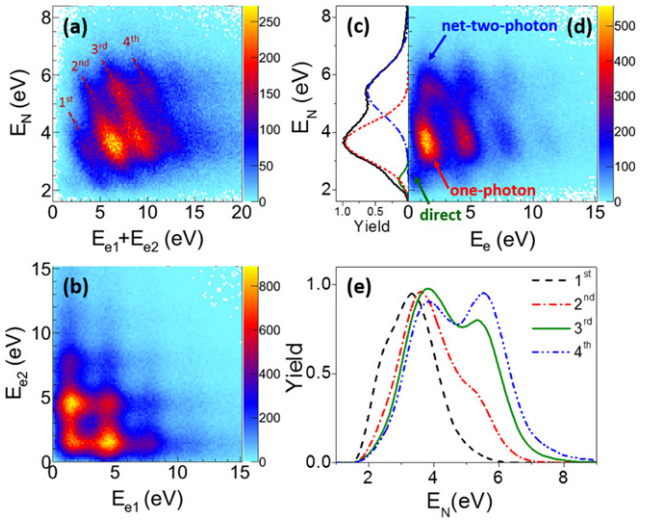


**Figure 8.** (a) Measured electron–nuclear JES of the sum energy of two protons. i.e., $E_N$, and sum energy of two electrons i.e., $E_{e1} + E_{e_2}$, of the ($H^+$, $H^+$) channel in linearly polarized UV pulses with intensity of $1.1 \times 10^{14}$ W cm$^{-2}$. (b) Electron–electron JES of two freed electrons of ($H^+$, $H^+$) channel. (c) Nuclear energy spectrum $E_N$ integrated over the electron energy $E_e$. (d) The JES of the nuclear energy $E_N$ versus the energy of one of the two electrons ($E_{e1}$ or $E_{e_2}$) of the ($H^+$, $H^+$) channel. The three different pathways, i.e., direct, one-photon, and net-two-photon pathways, towards the double ionization of $H_2$ are indicated by both the tilted arrows in (d) and fitted Gaussian distributions of $E_N$ in (c). (e) The nuclear energy spectra $E_N$ integrated over one of the first four diagonal lines as labeled in (a). Reprinted figure with permission from [52], Copyright 2017 by the American Physical Society.

## 5. Electron–nuclear correlation in above-threshold dissociative double ionization of molecules

Following the absorption of multiphoton energy, the laser-induced double ionization may occur, in which process two electrons are either released sequentially or stripped out in a nonsequential manner. As compared to the single ionization, the electron–electron correlation was expected in nonsequential above-threshold double ionization (ATDI) [74–77]. The exchanging and sharing of the absorbed photon energies among the two freed electrons have been experimentally observed in both atoms [78] and molecules [57] in compliance with the electron–electron correlation.

Considering the electron–nuclear correlation, it has been shown that the freed electron and its parent ion in the dissociative single ionization of molecules are closely coupled to each other in the ionization step, leading to the photon energy sharing among them [39–50, 52]. For the dissociative ATDI of $H_2$ molecules, two electrons and two nuclei are involved. It is possible that the two electrons do not directly correlated each other but are released sequentially. Even so, it was recently experimentally reported [52] that the photon energy sharing among four particles still holds in the multiphoton ATDI of $H_2$, where the correlation between the successively released two electrons is bridged by the nuclear motion via their interactions. It provides profound insights into the electron–nuclear correlation in strong-field dissociative double ionization of molecules.

Figure 8(a) shows the measured four-particle-coincidence electron–nuclear JES of the Coulomb-exploded double ionization channel of $H_2 + n\omega \rightarrow H^+ + H^+ + e_1 + e_2$ [denoted as ($H^+$, $H^+$) channel] in a linearly polarized intense UV femtosecond laser field. The yield of the ($H^+$, $H^+$) channel as a function of the sum energy of two electrons, i.e., $E_{e1} + E_{e_2}$, and the sum energy of two ions, i.e., $E_N$, are plotted in the JES. The characteristic feature of the electron–nuclear JES is the multiple energy conservation (diagonal) lines which evidently reflects the sharing of the absorbed photon energy among the ejected two electrons and two ions in the multiphoton ATDI of $H_2$ molecule.

Beyond the general photon energy sharing feature, the JES also allows to reveal the accessing dynamics of the dissociative double ionization of molecules. As shown in figure 8(b), the discrete islands appeared in the crossing of straight lines in the electron–electron JES of the ($H^+$, $H^+$) channel clearly indicate that the two electrons in the ATDI of $H_2$ molecule [52] are mostly sequentially released rather than via the nonsequential double ionization process [57, 78]. Moreover, as shown in figure 8(c), the nuclear kinetic energy $E_N$ of the ($H^+$, $H^+$) channel in the range of 2–8 eV is similar to that observed in the charge resonance enhanced double ionization of $H_2$ [21, 79, 80]. The generation of ($H^+$, $H^+$) channel can be described as a three-step process, as illustrated in figure 3. In the first step, the neutral $H_2$ is singly ionized by releasing an electron $e_1$ and $H_2^+$ in the $1s\sigma g$ state is formed. Secondly, the

ionization-created $H_2^+$ dissociates in the laser field via three different pathways, i.e., the direct pathway (direct dissociation without absorbing extra photons), one-photon pathway (absorbing one-photon when the molecular bond stretches to point B), or the net-two-photon pathway (propagation along the $1s\sigma g$ potential surface undergoing photon-coupled transition to the $2p\sigma u$ state by absorbing three photons at point A, followed by propagation along the $2p\sigma u$ surface and coupling back to the $1s\sigma g$ state by emitting one photon at point B, ended with the dissociation along the $1s\sigma g$ state). Thirdly, the dissociating $H_2^+$ is further ionized when the internuclear separation increase to the critical value for CREI, leaving behind two bare protons $H^+$ which repel each other. Interestingly, as shown in figure 8(d), three distinct sets of tilted strips with nuclear energy $E_N$ in the ranges of 2–3 eV, 3–5 eV, and 5–8 eV in the JES of one electron versus two nuclei of the ($H^+$, $H^+$) channel are observed, corresponding to the aforementioned three photon-resolved pathways towards the CREI of the stretching molecular ion of $H_2^+$.

Depending on the total number of photons absorbed by the molecule, the accessibility, enhancement, and suppression of various photon-resolved pathway is also observed in the ATDI of $H_2$ molecule [52]. As indicated by the dashed lines in figure 8(a), each diagonal line (ATI order) in the JES stands for a constant number of photons absorbed by the molecule. Figure 8(e) plots the corresponding nuclear energy spectra $E_N$ for the first four ATI orders. Interestingly, with the increase of the ATI orders, i.e., the total number of absorbed photons, the dissociation pathway with higher nuclear energy becomes accessible with increased relative yield. For instance, the ($H^+$, $H^+$) channel is dominated by the direct and one-photon pathways for the 1st ATI order, while the net-two-photon pathway becomes more prominent for the 2nd ATI order. The yield of the net-two-photon pathway gradually increases with the increase of the absorbed number of photons, which even exceeds the one-photon pathway for the 4th ATI order. Meanwhile, the direct pathway is somewhat suppressed as the ATI order increases. The competitions between the three photon-resolved pathways provide an interesting observation for investigating the role of photon energy absorption and deposition in determining the dynamics of molecules.

## 6. Rydberg states excitation in dissociative frustrated ionization of molecules

After conclusion of the intense laser pulses, rather than being ionized, it was reported that a fraction of the neutral atoms or molecules can survive in highly excited Rydberg states [23–26, 81–100]. For molecules exposed to strong laser fields, the excited Rydberg fragments can be formed in the process of molecular dissociative frustrated ionization. Taking the double ionization of molecules as an example, it is possible that one of the two liberated electrons does not escape to the continuum but is trapped to the high-lying Rydberg orbitals of the outgoing ionic fragments, leading to the dissociative frustrated double ionization (FDI) [23–26]. The Rydberg fragment formation in the dissociative FDI channel was generally observed in various molecular systems, such as $H_2$ [23, 24, 26], $D_2$ [25, 96], $N_2$ [88], $D_3^+$ [93, 94], CO [99], $CO_2$ [100] and clusters [88–91]. The dynamics of the dissociative FDI of hydrogen molecules has been real-time visualized using a few-cycle pump-probe scheme and the bond stretching of the molecular ion was identified to play a key role in the formation of the neutral Rydberg fragments [26, 96]. More recently, the strong-field Rydberg excitation was also explored in the dissociative frustrated single ionization of molecules by observing a neutral and an excited Rydberg nuclear fragments in the final reaction products [98]. Although the unexcited neutral fragment cannot be directly detected, the photon-excitation-created excited Rydberg fragments are measured with assistance of the postpulse static dc-field ionization, leading to the lowest order of the dissociative Rydberg fragmentation channel of molecules.

### *6.1. Multiphoton resonant excitation vs frustrated tunneling ionization*

Although the strong-field induced Rydberg state excitation has been extensively studied over the past, the underlying physical mechanism for the Rydberg fragments formation is yet a puzzle via the multiphoton resonant excitation [53, 81–84, 98] or frustrated tunneling ionization (FTI) [23–26, 85–97, 99, 100], where different experimental perspectives are expected. In the multiphoton scenario, the population of the Rydberg states is accessed via resonant multiphoton excitation which generally occurs when the potential energy of the highly excited state matches the photons. However, the FTI mechanism is viewed as an electron recapture picture. It attributes the formation of the Rydberg fragments to the recapturing of a tunneled electron by the ionic nucleus into a Rydberg orbital at the ends of the laser pulse.

In the previous experimental studies using a near-IR laser pulse, the dynamics of dissociative FDI of $H_2$ molecules [23, 26], i.e., $H_2 + n\omega \rightarrow H^+ + H^* + e_{freed}$ [denoted as ($H^+$, $H^*$) channel], was interpreted using the electron recapture picture of the FTI mechanism, which is supported by two significant features. One is that the ($H^+$, $H^*$) channel and Coulomb exploded double ionization channel ($H^+$, $H^+$) share comparable nuclear KER spectra since the ($H^+$, $H^+$) channel serves as the precursor for the electron-recapture-induced ($H^+$, $H^*$) channel. The other is that the ($H^+$, $H^*$) channel is favored in linearly polarized laser pulses but is suppressed in circularly polarized light in which the electron is driven away from the ionic cores and unable to be recaptured. However, in a recent experiment using a UV light [53], it was found that the KER spectrum of the nuclear fragments of ($H^+$, $H^*$) channel differs significantly from that of the ($H^+$, $H^+$) channel, as shown in figure 9(a), which is surprisingly in contrast to the previous observations using near-IR laser pulses [23]. Moreover, as displayed in figure 9(d), the ($H^+$, $H^*$) channel is clearly observed in the circularly polarized UV pulse, which again contradicts the FTI scenario.

From the theoretical point of view, according to the FTI scenario, the similarity of the nuclear KER spectra of the ($H^+$, $H^*$) and ($H^+$, $H^+$) channels in the near-IR laser pulses and the

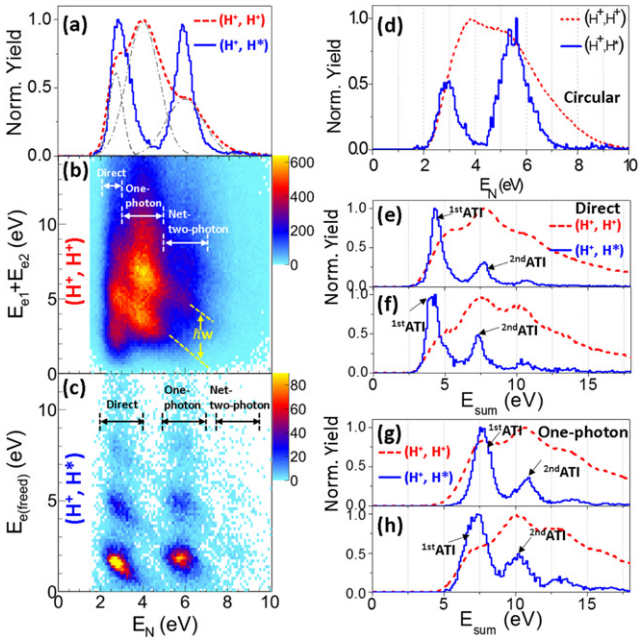


**Figure 9.** (a) Measured nuclear kinetic energy spectra $E_N$ of ($H^+$, $H^*$) (blue solid line) and ($H^+$, $H^+$) (red dashed line) channels in a linearly polarized UV (395 nm) laser pulse with peak intensity of $7.5 \times 10^{13}$ W cm$^{-2}$. (b) and (c) The corresponding electron–nuclear JES of the (b) ($H^+$, $H^+$) and (c) ($H^+$, $H^*$) channels. The three photon-resolved pathways towards breaking of $H_2$ molecules are indicated in the JES with $E_N$ in different ranges. (d) Measured $E_N$ spectra of the ($H^+$, $H^*$) (blue solid line) and ($H^+$, $H^+$) (red dashed line) channels driven by a circularly polarized UV laser pulse with intensity of $1.3 \times 10^{14}$ W cm$^{-2}$. (e)–(h) The $E_{sum}$ spectra of the freed electrons and nuclear fragments of the (e), (f) direct and (g), (h) one-photon pathway of the ($H^+$, $H^+$) and ($H^+$, $H^*$) channels driven by the linear UV laser pulse with intensities of (e), (g) $0.75 \times 10^{14}$ W cm$^{-2}$ and (f), (h) $1.0 \times 10^{14}$ W cm$^{-2}$. Adapted figures with permission from [53], copyright © 2019, Springer Nature.

suppression of the dissociative FDI in circularly polarized laser pulse can be well reproduced in the classical trajectory Monte Carto simulations [23, 24, 86, 93]. The theoretical treatment of FTI scenario is based on the two-step semi-classical model, i.e., the tunneling ionization followed by the classical propagation of the tunneled electron. From the calculations, the final momenta of the outgoing nuclear fragments and the principle quantum number $n$ of the excited fragments can be exactly extracted [23, 86]. Moreover, the developed three-dimensional semi-classical model [24, 94] allows for predicting two pathways for the electron trapping in ($H^+$, $H^*$) [24] which has stimulated further related experimental studies [96]. However, the classical simulation methods based on the FTI picture fails to predict the KER spectrum of the ($H^+$, $H^*$) channel in UV light, as shown in figure 9(a). A careful examination of the dissociative FDI dynamics based on accurate numerical solution of TDSE of $H_2$ molecule, of which however is not an easy task, might allow for reproducing the interesting features. By solving the TDSE of the hydrogen atom [83], the population of Rydberg states in strong laser fields is identified to be accessed via the multiphoton resonant excitation rather than the FTI.

To reveal a complete picture for the generation of Rydberg fragments in strong-field dissociation of molecules, the coincidence measurement of all the ejected electrons and nuclear fragments is crucial since the electron and nuclei are strongly coupled in molecules.

### *6.2. General of electron–nuclear correlated multiphoton scenario*

The complete measurement of the freed electrons, charged $H^+$ and excited neutral $H^*$ ejected from the ($H^+$, $H^*$) and ($H^+$, $H^+$) channels was performed using a reaction microscope [26, 96], which allows one to reveal the critical role of electron–nuclear correlation in the Rydberg state excitation in the dissociation of molecules [53]. Figures 9(b) and (c) present the measured electron–nuclear JES of the ($H^+$, $H^+$) and ($H^+$, $H^*$) channel in a linearly polarized UV light, respectively [53]. Interestingly, as shown in the JES, although the nuclear kinetic energy spectrum $E_N$ of the ($H^+$, $H^*$) channels is much different from that of the ($H^+$, $H^+$) channel, the aforementioned three photon-resolved pathways accessing for the ($H^+$, $H^+$) channel still exhibits in the ($H^+$, $H^*$) channel. It suggests that these two channels might be accessed via a comparable three-step process [52, 53]. It is confirmed by calculating the total energies $E_{sum}$ of all the ejected particles which are equal for the same pathway in these two channels since the electrons and nuclei of the molecule as a whole absorbs the photon energy. Figures 9(e) and (g) plot the $E_{sum}$ spectra of ($H^+$, $H^*$) and ($H^+$, $H^+$) channels accessed via the direct and one-photon pathways, respectively. The well-matched locations of the discrete ATI peaks in the $E_{sum}$ spectra for these two channels indicate that, for a given photon-resolved pathway, the $H_2$ molecule absorbs the same number of photons in producing these two different channels.

The observed distinct $E_N$ spectra of the ($H^+$, $H^*$) and ($H^+$, $H^+$) channels are ascribed to the different energy partition laws among the electrons and nuclei. For the ($H^+$, $H^+$) channel, the freed electrons mostly take the absorbed photon energy exceeding the double ionization threshold. This excess photon energy is deposited into the outgoing nuclei of the ($H^+$, $H^*$) channel by resonantly populating the repulsive Rydberg states at a smaller internuclear distance, which leads to a relatively higher kinetic energy of the nuclear fragments of the ($H^+$, $H^*$) channel as compared to that of the ($H^+$, $H^+$) channel. More interestingly, the photon energy sharing among the ejected electron and nuclear fragments of the ($H^+$, $H^*$) channel is altered by the laser-induced ac-Stark shift. By considering the intensity-dependent Stark shift of the ionization threshold, as shown in figures 9(e)–(h), the energy of the first and second ATI peaks of the $E_{sum}$ spectrum will shift towards the low energy as the laser intensity increases. Due to the different energy partition laws between the ($H^+$, $H^*$) and ($H^+$, $H^+$) channels, the laser-intensity dependent shifts of the $E_{sum}$ are also manifested in the energy shift of the $E_N$ spectrum of ($H^+$, $H^*$) channel. With the increase of the laser intensity, the internuclear distance for the multiphoton resonant excitation becomes larger due to the uprising of the potential energy of the excited Rydberg states. It leads to the shifting of the nuclear kinetic energy of ($H^+$, $H^*$) channel for each pathway towards the low energy, as shown in figures 10(a)–(d).

More interestingly, the accessibilities of the high-order photon-resolved pathways increases with the laser intensity.

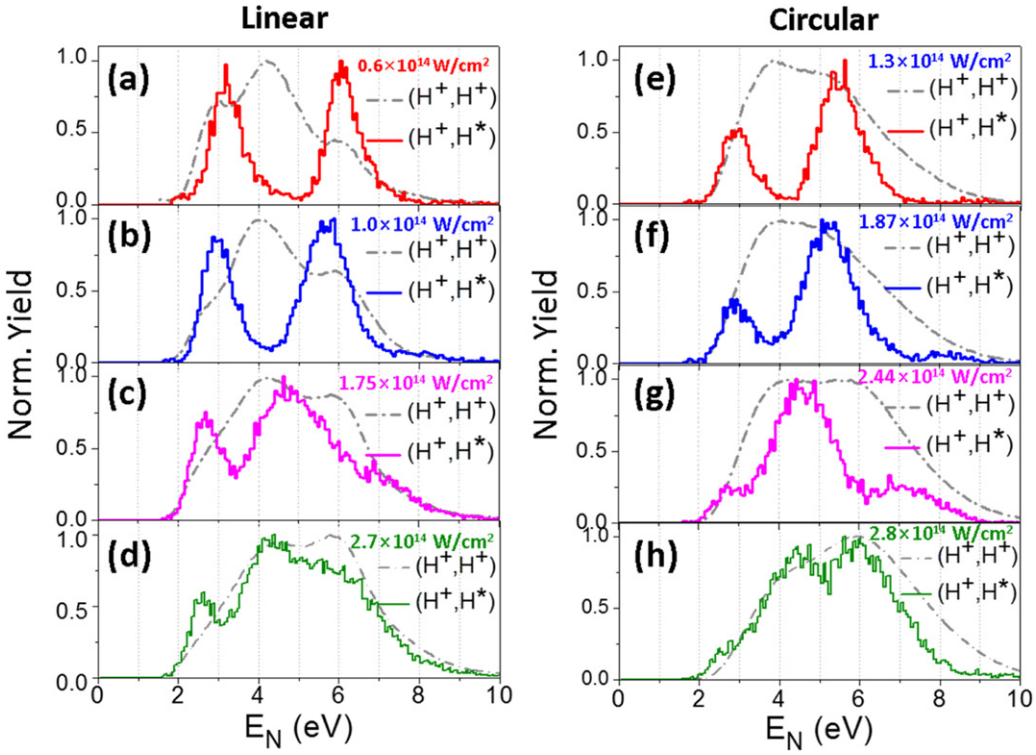


**Figure 10.** Measured nuclear kinetic energy spectra $E_N$ of the ($H^+$, $H^+$) and ($H^+$, $H^*$) channels driven by (a)–(d) linearly polarized and (e)–(h) circularly polarized UV pulses at various laser intensities. Adapted figures with permission from [53], copyright © 2019, Springer Nature.

When the laser intensity increases up to a certain value, the $E_N$ spectrum of the ($H^+$, $H^*$) channel resembles that of the ($H^+$, $H^+$) channel. It is consistent with the observations using near-IR laser pulses which is generally explained by the electron recapture picture [23]. Actually, for longer wavelength, the photon energy is smaller and the corresponding $U_p$ shift is larger. As a result, the three energy peaks induced by the three photon-resolved pathways are broadened and overlap with each other and thus the $E_N$ spectrum of the ($H^+$, $H^*$) channel becomes similar to that of the ($H^+$, $H^+$) channel as the FTI scenario expected. Therefore, the multiphoton-route with intrinsic electron–nuclear correlation is the general mechanism in producing Rydberg fragments in strong-field dissociative ionization of molecules, which can also explain the observation of the FTI scenario at long laser wavelengths. An additional solid evidence of the multiphoton-route to the Rydberg fragments of molecules is that the intensity-dependent $E_N$ spectra of ($H^+$, $H^*$) channel are also observed in circularly polarized UV pulses, as shown in figures 10(e)–(h). For the ($H^+$, $H^*$) channel in circularly polarized near-IR laser fields [23], the cross section for the resonant excitation is relatively lower since more photons are required, thus leading to a much less accessibility of the Rydberg fragments as compared to the UV lasers. Moreover, the electron–nuclear correlated multiphoton resonant excitation is also responsible for the formation of Rydberg fragments in the dissociative frustrated single ionization of molecules [98], which further verifies the general of the multiphoton-route to Rydberg fragments of molecules.

## 7. Conclusion and outlook

The electronic and nuclear motions inside a molecule are of fundamental importance in determining the ultrafast physicochemical reactions. Although the electron is several orders in magnitude lighter than the nuclei, their motions are generally coupled with each other, which plays a crucial role in strong-field dynamics of molecules. In this article, we have reviewed recent progresses of the electron–nuclear correlated dynamics of molecules exposed to strong laser fields, in particular, the photon energy absorption and deposition as the primary stage of the light–molecule interactions. In the strong-field dissociative ionization of molecules, two essential questions of how the molecule absorbs the photon energy and how the energy is distributed among the subsystems of the molecules are answered by means of the electron–nuclear JES. When the molecule coherently absorbs multiple photons from the laser fields, the nature of photon energy sharing among the electrons and nuclei of the molecule is revealed by the multiple diagonal lines in the JES. Each line indicates that the electrons and nuclei of the molecule as a whole absorbs the photon energy. The electron–nuclear correlated photon energy sharing dynamics is generally observed in the dissociative single and double ionization of molecules, where the electron–nuclear correlation is bridged by the interplay of the electronic and nuclear motions. The prerequisite for the electron–nuclear energy sharing is the population of numerous vibrational states of the molecular ions in the ionization process. It serves as the energy reservoir for the nuclei

storing the shared photon energy. Differing from the simplest one- or two-electron molecules, electron–nuclear photon energy sharing dynamics in the multi-electronic molecules is altered when various molecular orbitals participate in the dissociative ionization process. It offers a perspective to reveal the fingerprints of the multi-orbital effects in the molecular processes and further decode the underlying attosecond multi-electron dynamics [101].

Beyond revealing the correlated photon energy sharing dynamics, the electron–nuclear JES is also useful for exploring richer fundamental molecular processes where the multiparticle correlation plays key roles. Basing on the coincidence measurements of all the ejected particles of a breaking molecule, the interesting strong-field phenomena of photon-number-dependent asymmetric dissociative single ionization, high-order ATD and resonant multiphoton-route to Rydberg fragments of molecules are unveiled. Understanding of various strong-field molecular dynamics from the perspective of the electron–nuclear correlation would open the possibilities to manipulate the dynamics of the electrons or nuclei via one of them and thus determine the ultimate fate of the molecules.

The electron–nuclear correlated dynamics in dissociative ionization of a molecule appears inevitably associated with the bond stretching of the molecular ion. The recently proposed ultrafast stopwatch strategy using polarization-skewed laser pulses makes the observation of bond stretching of the molecular dissociation experimentally accessible [102]. It provides a straightforward and robust way to probe the correlated electronic and nuclear dynamics in the dissociative ionization of molecule with sub-cycle time resolution. Moreover, the advent of attosecond science [103, 104] has enabled the investigation of the light-induced electronic and nuclear dynamics in real-time. The attosecond electron–nuclear correlated dynamics has been demonstrated using an advanced IR-pump and extreme-ultraviolet (XUV)-probe spectroscopic method [105]. Nowadays, the atto-COLTRIMS apparatus consisting of XUV pulses with attosecond time resolution and a reaction microscope allowing for full particles coincidence detection is developing. It has illuminated the future works on time-resolving the electron–nuclear correlated dynamics in molecules and imaging the electronic and nuclear wave packet during the chemical reactions.

## Acknowledgments

We would like to acknowledge many coworkers and colleagues who have contributed to the research results described in this review. This work is supported by the National Key R & D Program of China (2018YFA0306303), the National Natural Science Fund (Grants Nos. 11761141004, 11834004, 11704124), the 111 Project of China (Grant No. B12024), Projects from Shanghai Science and Technology Commission (19JC1412200, 19ZR1473900), and the Shanghai Sailing Program (Grant No. 17YF1404000). WZ acknowledges the supports from the Outstanding Doctoral Dissertation Cultivation Plan of Action (YB2016036) and the Future Scientist Cultivation Program of ECNU.

## ORCID iDs

Wenbin Zhang https://orcid.org/0000-0001-9726-2282
Xiaochun Gong https://orcid.org/0000-0002-4826-6049
Jian Wu https://orcid.org/0000-0002-1318-2291

## References

[1] Zewail A H 1988 Laser femtochemistry *Science* **242** 1645
[2] Krausz F and Ivanov M 2009 Attosecond physics *Rev. Mod. Phys.* **81** 163
[3] Bucksbaum P H *et al* 1990 Softening of the $H_2^+$ molecular bond in intense laser fields *Phys. Rev. Lett.* **64** 1883
[4] Frasinski L J *et al* 1999 Manipulation of bond hardening in $H_2^+$ by chirping of intense femtosecond laser pulses *Phys. Rev. Lett.* **83** 3625
[5] Yao G and Chu S-I 1993 Molecular-bond hardening and dynamics of molecular stabilization and trapping in intense laser pulses *Phys. Rev.* A **48** 485
[6] Bandrauk A D and Sink M L 1981 Photodissociation in intense laser fields: predissociation analogy *J. Chem. Phys.* **74** 1110
[7] Giusti-Suzor A, He X, Atabek O and Mies F H 1990 Above-threshold dissociation of $H_2^+$ in intense laser fields *Phys. Rev. Lett.* **64** 515
[8] Jolicard G and Atabek O 1992 Above-threshold-dissociation dynamics of $H_2^+$ with short intense laser pulses *Phys. Rev.* A **46** 5845
[9] Orr P A *et al* 2007 Above threshold dissociation of vibrationally cold $HD^+$ molecules *Phys. Rev. Lett.* **98** 163001
[10] McKenna J *et al* 2008 Enhancing high-order above-threshold dissociation of $H_2^+$ beams with few-cycle laser pulses *Phys. Rev. Lett.* **100** 133001
[11] Li Z C, Ruiz C and He F 2014 Tunneling dissociation of $H_2^+$ and its isotopes in THz laser pulses *Phys. Rev.* A **90** 033421
[12] Kling M F *et al* 2006 Control of electron localization in molecular dissociation *Science* **312** 246
[13] Wu J *et al* 2013 Understanding the role of phase in chemical bond breaking with coincidence angular streaking *Nat. Commun.* **4** 2177
[14] Meckel M *et al* 2008 Laser-induced electron tunneling and diffraction *Science* **320** 1478
[15] Blaga C I *et al* 2012 Imaging ultrafast molecular dynamics with laser-induced electron diffraction *Nature* **483** 194
[16] Pullen M G *et al* 2015 Imaging an aligned polyatomic molecule with laser-induced electron diffraction *Nat. Commun.* **6** 7262
[17] Krause J L, Schafer K J and Kulander K C 1992 High-order harmonic generation from atoms and ions in the high intensity regime *Phys. Rev. Lett.* **68** 3535
[18] Kraus P M, Rupenyan A and Wörner H J 2012 High-harmonic spectroscopy of oriented OCS molecules: emission of even and odd harmonics *Phys. Rev. Lett.* **109** 233903
[19] Zuo T and Bandrauk A D 1995 Charge-resonance-enhanced ionization of diatomic molecular ions by intense lasers *Phys. Rev.* A **52** R2511
[20] Seideman T, Ivanov M Y and Corkum P B 1995 Role of electron localization in intense-field molecular ionization *Phys. Rev. Lett.* **75** 2819
[21] Chelkowski S *et al* 2007 Dynamic nuclear interference structures in the Coulomb explosion spectra of a hydrogen molecule in intense laser fields: reexamination of molecular enhanced ionization *Phys. Rev.* A **76** 013405
[22] Wu J, Meckel M, Schmidt L P H, Kunitski M, Voss S, Sann H, Kim H, Jahnke T, Czasch A and Dörner R 2012 Probing the tunnelling site of electrons in strong field enhanced ionization of molecules *Nat. Commun.* **3** 1113

[23] Manschwetus B *et al* 2009 Strong laser field fragmentation of $H_2$: Coulomb explosion without double ionization *Phys. Rev. Lett.* **102** 113002

[24] Emmanouilidou A *et al* 2012 Routes to formation of highly excited neutral atoms in the breakup of strongly driven $H_2$ *Phys. Rev.* A **85** 011402

[25] McKenna J *et al* 2011 Frustrated tunneling ionization during laser-induced $D_2$ fragmentation: detection of excited metastable $D^*$ atoms *Phys. Rev.* A **84** 043425

[26] Zhang W *et al* 2017 Visualizing and steering dissociative frustrated double ionization of hydrogen molecules *Phys. Rev. Lett.* **119** 253202

[27] Sánchez I and Martín F 1997 Origin of unidentified structures in resonant dissociative photoionization of $H_2$ *Phys. Rev. Lett.* **79** 1654

[28] Martín F *et al* 2007 Single photon-induced symmetry breaking of $H_2$ dissociation *Science* **315** 629

[29] Gagnon E, Ranitovic P, Tong X M, Cocke C L, Murnane M M, Kapteyn H C and Sandhu A S 2007 Soft x-ray-driven femtosecond molecular dynamics *Science* **317** 1374

[30] Zhou X, Ranitovic P, Hogle C W, Eland J H D, Kapteyn H C and Murnane M M 2012 Probing and controlling non-Born–Oppenheimer dynamics in highly excited molecular ions *Nat. Phys.* **8** 232–7

[31] Silva R E F, Rivière P and Martín F 2012 Autoionizing decay of $H_2$ doubly excited states by using xuv-pump–infrared-probe schemes with trains of attosecond pulses *Phys. Rev.* A **85** 063414

[32] Tolstikhin O I and Madsen L B 2013 Retardation effects and the Born-Oppenheimer approximation: theory of tunneling ionization of molecules revisited *Phys. Rev. Lett.* **111** 153003

[33] Mi Y, Camus N, Fechner L, Laux M, Moshammer R and Pfeifer T 2017 Electron-nuclear coupling through autoionizing states after strong-field excitation of $H_2$ molecules *Phys. Rev. Lett.* **118** 183201

[34] Ullrich J *et al* 2003 Recoil-ion and electron momentum spectroscopy: reaction-microscopes *Rep. Prog. Phys.* **66** 1463

[35] Dörner R *et al* 2000 Cold target recoil ion momentum spectroscopy: a 'momentum microscope' to view atomic collision dynamics *Phys. Rep.* **330** 95

[36] Lafosse A *et al* 2000 Vector correlations in dissociative photoionization of diatomic molecules in the VUV range: strong anisotropies in electron emission from spatially oriented NO molecules *Phys. Rev. Lett.* **84** 5987

[37] Osipov T *et al* 2008 Fragmentation pathways for selected electronic states of the acetylene dication *J. Phys. B: At. Mol. Opt. Phys.* **41** 091001

[38] Agostini P, Fabre F, Mainfray G, Petite G and Rahman N K 1979 Free-free transitions following six-photon ionization of xenon atoms *Phys. Rev. Lett.* **42** 1127

[39] Madsen C B, Anis F, Madsen L B and Esry B D 2012 Multiphoton above threshold effects in strong-field fragmentation *Phys. Rev. Lett.* **109** 163003

[40] Silva R E F, Catoire F, Rivière P, Bachau H and Martín F 2013 Correlated electron and nuclear dynamics in strong field photoionization of $H_2^+$ *Phys. Rev. Lett.* **110** 113001

[41] Yue L and Madsen L B 2013 Dissociation and dissociative ionization of $H_2^+$ using the time-dependent surface flux method *Phys. Rev.* A **88** 063420

[42] Liu K L, Lan P F, Huang C, Zhang Q B and Lu P X 2014 Revealing correlated electronic and nuclear dynamics in molecules with energy-resolved population imaging *Phys. Rev.* A **89** 053423

[43] Catoire F *et al* 2014 Molecular resolvent-operator method: electronic and nuclear dynamics in strong-field ionization *Phys. Rev.* A **89** 023415

[44] Mosert V and Bauer D 2015 Dissociative ionization of $H_2^+$: few-cycle effect in the joint electron-ion energy spectrum *Phys. Rev.* A **92** 043414

[45] Wang Z *et al* 2016 Counterintuitive energy shifts in joint electron–nuclear-energy spectra of strong-field fragmentation of $H_2^+$ *Phys. Rev.* A **93** 013418

[46] Yue L and Madsen L B 2016 Inter- and intracycle interference effects in strong-field dissociative ionization *Phys. Rev.* A **93** 031401

[47] Wu J *et al* 2013 Electron-nuclear energy sharing in above-threshold multiphoton dissociative ionization of H2 *Phys. Rev. Lett.* **111** 023002

[48] Zhang W *et al* 2016 Photon energy deposition in strong-field single ionization of multielectron molecules *Phys. Rev. Lett.* **117** 103002

[49] Sun X, Li M, Shao Y, Liu M-M, Xie X, Deng Y, Wu C, Gong Q and Liu Y 2016 Vibrationally resolved electron-nuclear energy sharing in above-threshold multiphoton dissociation of CO *Phys. Rev.* A **94** 013425

[50] Zhang W *et al* 2017 Photon-number-resolved asymmetric dissociative single ionization of $H_2$ *Phys. Rev.* A **96** 033405

[51] Lu P *et al* 2018 High-order above-threshold dissociation of molecules *Proc. Natl Acad. Sci. USA* **115** 2049

[52] Lu P, Zhang W, Gong X, Song Q, Lin K, Ji Q, Ma J, He F, Zeng H and Wu J 2017 Electron-nuclear correlation in above-threshold double ionization of molecules *Phys. Rev.* A **95** 033404

[53] Zhang W *et al* 2019 Electron-nuclear correlated multiphoton-route to Rydberg fragments of molecules *Nat. Commun.* **10** 757

[54] Feuerstein B and Thumm U 2003 Fragmentation of $H_2^+$ in strong 800-nm laser pulses: initial-vibrational-state dependence *Phys. Rev.* A **67** 043405

[55] Freeman R R, Bucksbaum P H, Milchberg H, Darack S, Schumacher D and Geusic M E 1987 Above-threshold ionization with subpicosecond laser pulses *Phys. Rev. Lett.* **59** 1092

[56] Bucksbaum P H, Van Woerkom L D, Freeman R R and Schumacher D W 1990 Nonresonant above-threshold ionization by circularly polarized subpicosecond pulses *Phys. Rev.* A **41** 4119

[57] Gong X *et al* 2015 Channel-resolved above-threshold double ionization of acetylene *Phys. Rev. Lett.* **114** 163001

[58] Kremer M *et al* 2009 Electron localization in molecular fragmentation of $H_2$ by carrier-envelope phase stabilized laser pulses *Phys. Rev. Lett.* **103** 213003

[59] Fischer B *et al* 2010 Steering the electron in $H_2^+$ by nuclear wave packet dynamics *Phys. Rev. Lett.* **105** 223001

[60] Znakovskaya I *et al* 2012 Subcycle controlled charge-directed reactivity with few-cycle midinfrared pulses *Phys. Rev. Lett.* **108** 063002

[61] Rathje T *et al* 2013 Coherent control at its most fundamental: carrier-envelope-phase-dependent electron localization in photodissociation of a $H_2^+$ molecular ion beam target *Phys. Rev. Lett.* **111** 093002

[62] Kling N G *et al* 2013 Carrier-envelope phase control over pathway interference in strong-field dissociation of $H_2^+$ *Phys. Rev. Lett.* **111** 163004

[63] Xu H *et al* 2017 Observing electron localization in a dissociating $H_2^+$ molecule in real time *Nat. Commun.* **8** 15849

[64] Charron E, Giusti-Suzor A and Mies F H 1993 Two-color coherent control of $H_2^+$ photodissociation in intense laser fields *Phys. Rev. Lett.* **71** 692

[65] Sheehy B, Walker B and DiMauro L F 1995 Phase control in the two-color photodissociation of $HD^+$ *Phys. Rev. Lett.* **74** 4799

[66] Ohmura H, Saito N and Tachiya M 2006 Selective ionization of oriented nonpolar molecules with asymmetric structure

by phase-controlled two-color laser fields *Phys. Rev. Lett.* **96** 173001
[67] Ray D *et al* 2009 Ion-energy dependence of asymmetric dissociation of $D_2$ by a two-color laser field *Phys. Rev. Lett.* **103** 223201
[68] Wu J *et al* 2013 Comparison of dissociative ionization of $H_2$, $N_2$, $Ar_2$, and CO by elliptically polarized two-color pulses *Phys. Rev.* A **87** 023406
[69] Wanie V *et al* 2016 Coherent control of D2/H2 dissociative ionization by a mid-infrared two-color laser field *J. Phys. B: At. Mol. Opt. Phys.* **49** 025601
[70] Gong X *et al* 2014 Two-dimensional directional proton emission in dissociative ionization of $H_2$ *Phys. Rev. Lett.* **113** 203001
[71] Song Q *et al* 2015 Directional deprotonation ionization of acetylene in asymmetric two-color laser fields *J. Phys. B: At. Mol. Opt. Phys.* **48** 094007
[72] Lin K *et al* 2016 Directional bond breaking by polarization-gated two-color ultrashort laser pulses *J. Phys. B: At. Mol. Opt. Phys.* **49** 025603
[73] Roudnev V and Esry B D 2007 General theory of carrier-envelope phase effects *Phys. Rev. Lett.* **99** 220406
[74] Lein M, Gross E K U and Engel V 2001 Discrete peaks in above-threshold double-ionization spectra *Phys. Rev.* A **64** 023406
[75] Parker J S, Doherty B J S, Taylor K T, Schultz K D, Blaga C I and DiMauro L F 2006 High-energy cutoff in the spectrum of strong-field nonsequential double ionization *Phys. Rev. Lett.* **96** 133001
[76] Liao Q and Lu P 2010 Energy correlation in above-threshold nonsequential double ionization at 800 nm *Phys. Rev.* A **82** 021403
[77] Armstrong G S J, Parker J S and Taylor K T 2011 Double-electron above-threshold ionization resonances as interference phenomena *New J. Phys.* **13** 013024
[78] Henrichs K *et al* 2013 Observation of electron energy discretization in strong field double ionization *Phys. Rev. Lett.* **111** 113003
[79] Esry B D, Sayler A M, Wang P Q, Carnes K D and Ben-Itzhak I 2006 Time-resolved imaging and manipulation of $H_2$ fragmentation in intense laser fields *Phys. Rev. Lett.* **97** 013003
[80] Ergler T, Rudenko A, Feuerstein B, Zrost K, Schröter C D, Moshammer R and Ullrich J 2005 Time-resolved imaging and manipulation of $H_2$ fragmentation in intense laser fields *Phys. Rev. Lett.* **95** 093001
[81] Boer M P de and Muller H G 1992 Observation of large populations in excited states after short-pulse multiphoton ionization *Phys. Rev. Lett.* **68** 2747
[82] Jones R R, Schumacher D W and Bucksbaum P H 1993 Population trapping in Kr and Xe in intense laser fields *Phys. Rev.* A **47** R49
[83] Li Q *et al* 2014 Fine structures in the intensity dependence of excitation and ionization probabilities of hydrogen atoms in intense 800-nm laser pulses *Phys. Rev.* A **89** 023421
[84] Gibson G N, Fang L and Moser B 2006 Direct femtosecond laser excitation of the 2p state of H by a resonant seven-photon transition in $H_2^+$ *Phys. Rev.* A **74** 041401
[85] Wang B B, Li X F, Fu P M, Chen J and Liu J 2006 Coulomb potential recapture effect in above-barrier ionization in laser pulses *Chin. Phys. Lett.* **23** 2729
[86] Nubbemeyer T, Gorling K, Saenz A, Eichmann U and Sandner W 2008 Strong-field tunneling without ionization *Phys. Rev. Lett.* **101** 233001
[87] Eichmann U, Nubbemeyer T, Rottke H and Sandner W 2009 Acceleration of neutral atoms in strong short-pulse laser fields *Nature* **461** 1261
[88] Nubbemeyer T *et al* 2009 Excited neutral atomic fragments in the strong-field dissociation of $N_2$ molecules *J. Phys. B: At. Mol. Opt. Phys.* **42** 134010
[89] Ulrich B *et al* 2010 Double-ionization mechanisms of the argon dimer in intense laser fields *Phys. Rev.* A **82** 013412
[90] Manschwetus B *et al* 2010 Mechanisms underlying strong-field double ionization of argon dimer *Phys. Rev.* A **82** 013413
[91] Wu J *et al* 2011 Multiple recapture of electrons in multiple ionization of the argon dimer by a strong laser field *Phys. Rev. Lett.* **107** 043003
[92] Xie X, Wu C, Liu H, Li M, Deng Y, Liu Y, Gong Q and Wu C 2013 Tunneling electron recaptured by an atomic ion or a molecular ion *Phys. Rev.* A **88** 065401
[93] McKenna J, Sayler A M, Gaire B, Kling N G, Esry B D, Carnes K D and Itzhak I B 2012 Frustrated tunnelling ionization during strong-field fragmentation of $D_3^+$ *New J. Phys.* **14** 103029
[94] Chen A, Price H, Staudte A and Emmanouilidou A 2016 Frustrated double ionization in two-electron triatomic molecules *Phys. Rev.* A **94** 043408
[95] Lv H *et al* 2016 Comparative study on atomic and molecular Rydberg-state excitation in strong infrared laser fields *Phys. Rev.* A **93** 033415
[96] Zhang W *et al* 2018 Tracking the electron recapture in dissociative frustrated double ionization of $D_2$ *Phys. Rev.* A **98** 013419
[97] Larimian S *et al* 2017 Coincidence spectroscopy of high-lying Rydberg states produced in strong laser fields *Phys. Rev.* A **96** 021403
[98] Ma J *et al* 2019 Strong-field dissociative Rydberg excitation of oxygen molecules: electron-nuclear correlation *Phys. Rev.* A **98** 013419
[99] Zhang W *et al* 2020 Electron trapping in strong-field dissociative frustrated ionization of CO molecules *Phys. Rev.* A **101** 033401
[100] Hu H *et al* 2019 Laser-induced dissociative recombination of carbon dioxide *Phys. Rev. Res.* **1** 033152
[101] Smirnova O, Mairesse Y, Patchkovskii S, Dudovich N, Villeneuve D, Corkum P and Lvanov M Y 2009 High harmonic interferometry of multi-electron dynamics in molecules *Nature* **460** 972
[102] Ji Q *et al* 2019 Timing dissociative ionization of $H_2$ using a polarization-skewed femtosecond laser pulse *Phys. Rev. Lett.* **123** 233202
[103] Sansone G *et al* 2006 Isolated single-cycle attosecond pulses *Science* **314** 443–6
[104] Popmintchev T, Chen M C, Arpin P, Murnane M M and Kapteyn H C 2010 The attosecond nonlinear optics of bright coherent X-ray generation *Nat. Photon.* **4** 822–32
[105] Cattaneo L *et al* 2018 Attosecond coupled electron and nuclear dynamics in dissociative ionization of H2 *Nat. Phys.* **14** 733–8